Electron transfer properties of rhodium(I) oxalate complexes

J. E. Anderson* and C. P. Murphy
Department of Chemistry, Boston College, Chestnut Hill, MA 02167 (USA)
J. Real, J. Balué and J. C. Bayón*
Departament de Química, Universitat Autònoma de Barcelona, Bellaterra, 08193 Barcelona (Spain)

(Received October 20, 1992; revised March 17, 1993)

Abstract

The synthesis, electrochemical and spectroelectrochemical properties of (TMA)[Rh(ox)$(CO)_2$], (TMA)[Rh(ox)(COD)] and [Rh_2(ox)$(COD)_2$], where TMA is tetramethylammonium, COD is 1,5-cyclooctadiene and ox is oxalate dianion, are reported. The monometallic complexes, (TMA)[Rh(ox)$(CO)_2$] and (TMA)[Rh(ox)(COD)], can be oxidized by two electrons. However their oxidation is followed by a chemical reaction to form a solvated Rh complex and two equivalents of CO_2 due to decomposition of the oxalate. The bimetallic complex, [Rh_2(ox)$(COD)_2$], is oxidized electrochemically in two successive two-electron steps without decomposition of the coordinated oxalate. An equilibrium reaction between [Rh(ox)(COD)]$^-$, [Rh(COD)$(CH_3CN)_2$]$^+$ and [$Rh_2(COD)_2$(ox)] is present which complicates the electron transfer mechanism. Chemical oxidations of (TMA)[Rh(ox)(COD)] and [Rh_2(ox)$(COD)_2$] were performed to further establish the products of the oxidation reactions and the formation of [$Rh_2(CH_3CN)(COD)_2$(ox)]BF_4 is reported.

Introduction

As part of an investigation of the electron transfer properties of selected rhodium and iridium complexes [1], we wish to report the electrochemical and spectroelectrochemical properties of (TMA)[Rh(ox)$(CO)_2$], (TMA)[Rh(ox)(COD)] and [Rh_2(ox)$(COD)_2$], where COD is 1,5-cyclooctadiene. The synthesis and molecular structure of the d^8, square planar Rh(I) complex (TMA)[Rh(ox)$(CO)_2$], where TMA is tetramethylammonium cation and ox is the oxalate dianion, were recently reported by one of us [2]. This complex, in the solid state, consists of nearly linear chains of metal atoms with an equal rhodium–rhodium distance of 3.24 Å. Consistent with the crystal structure, (TMA)[Rh(ox)$(CO)_2$] exhibits dichroic properties, indicative of weak metal–metal interactions [3–6]. The COD eliminates the planarity of (TMA)[Rh(ox)(COD)] and [Rh_2(ox)$(COD)_2$] and hence the possibility for extended intermolecular metal–metal interactions. However, [Rh_2(ox)$(COD)_2$] is a bimetallic, oxalate bridged complex that has the possibility of intramolecular metal–metal interactions.

Reductive electrochemical data and molecular orbital calculations have been reported for the d^8 complexes, M(ox)$(PR_3)_2$ where M is Pt or Pd and PR_3 is trimethyl or triethylphosphine [7]. SCF-X_α-DV calculations on Pd(ox)$(PH_3)_2$ found the highest occupied molecular orbital (HOMO) to primarily exist on the oxalate ligand and the lowest unoccupied molecular orbital (LUMO) to consist of metal and oxalate orbitals. Compounds such as M(ox)$(PR_3)_2$ have the ability to undergo thermally or photochemically induced reductive elimination of oxalate to form Pd$(PR_3)_2$ and two equivalents of CO_2 [8]. Similarly, photochemically induced reductive elimination of oxalate from the d^6 species (Cp*)Ir(ox)$(PMe_3)_2$ is followed by an oxidative addition reaction with either the coordinated PMe_3 or a solvent molecule [9]. Such photochemical processes are reported with other non-d^8 transition metal oxalate systems as well [10, 11].

The use of transition metals to initiate and/or facilitate the oxidatively induced decomposition of oxalate to CO_2 is well known. For example, the standardization reaction of permanganate solutions with sodium oxalate is based on the oxidation of oxalate to CO_2 [12]. Similarly, formation of a bis(oxalate)–chromium complex prior to electron transfer is reported when oxalic acid is oxidized by chromium(VI) species [13], with the ultimate formation of CO_2 and reduced chromium species [14, 15]. The homogeneous, one-electron oxidation of oxalate generates CO_2 and the anion radical $(CO_2^{\cdot})^-$ and hence oxalate is often used in kinetic studies as a reducing

*Authors to whom correspondence should be addressed.

0020-1693/93/$6.00

agent [16, 17]. The standard potential of 0.475 V versus NHE is reported for the two-electron oxidation of oxalic acid to give two equivalents of CO_2 [18] in an aqueous solvent system.

Experimental

Equipment and techniques

Electrochemical experiments were performed with either a BAS-100A or an EG&G Princeton Applied Research 273 potentiostat/galvanostat coupled to an EG&G Princeton Applied Research model RE0091-XY recorder and an IBM PS/2 model 50 computer. A platinum button working electrode, approximate area 0.004 cm^2, a platinum wire counter electrode and an SCE reference electrode separated from the solution with a bridge, comprised the three-electrode system. All potentials are reported versus the SCE electrode and have a precision of 0.010 V. The ferrocene/ferrocenium couple was also used as an internal standard. The concentration of supporting electrolyte was 0.2 M unless otherwise stated.

Electronic spectroelectrochemical data were recorded with a Perkin-Elmer Lambda 3B UV–Vis spectrometer, interfaced to an IBM PS/2 model 60 computer with PECSS software, using a BAS CV-27 potentiostat coupled to an IBM 7427 MT X-Y-T recorder to monitor the current output. IR spectroelectrochemical data were recorded with a Nicolet 510 FT-IR spectrometer using the same electrochemical apparatus. The electrodes in the spectroelectrochemical cell are a large platinum minigrid working electrode, a platinum wire counter electrode and a platinum wire pseudo-reference electrode. The supporting electrolyte concentration was 0.2 M unless otherwise stated. A background subtraction to account for the presence of the electrode (with 50% transmittance) and the tail of the solvent absorbance band was performed with the UV–Vis data. The IR results are presented as difference spectra and consequently these effects are also removed.

The electrochemical cells are all home built and are designed for analysis of air sensitive species [19, 20]. All solid and solution transfers were carried out by standard Schlenk methodologies [21]. Conventional UV–Vis and IR measurements were performed with cells designed for inert atmosphere measurements. In addition to the above, IR spectra were also recorded with a Perkin-Elmer 1710 FT spectrometer. NMR spectra were recorded on a Bruker 400 MHz instrument. Chemical shifts are reported relative to TMS.

Materials

The acetonitrile (CH_3CN) and tetrahydrofuran (THF) used for electroanalysis were purchased (Aldrich) as spectroscopic grade, purified and dried by standard methods [22] and stored over calcium hydride (CH_3CN) or sodium/benzophenone (THF) under an inert atmosphere and distilled just prior to use. Tetrabutylammonium perchlorate (TBAP) and tetrabutylammonium tetrafluoroborate [TBA(BF_4)] were purchased from Fluka and Aldrich, respectively, doubly recrystallized from ethanol and dried in a vacuum oven at 50 °C. [$Rh_2(\mu\text{-}Cl)_2(COD)_2$] and [$Rh_2(\mu\text{-}OCH_3)_2(COD)_2$] were synthesized by published methods [23], carbon monoxide, oxalic acid ($H_2C_2O_4 \cdot 2H_2O$) and tetramethylammonium hydroxide [(TMA)OH] were purchased and used without further purification.

Metal complexes and their oxidation reactions

The complexes TMA[Rh(ox)$(CO)_2$], TMA[Rh(ox)(COD)] and the bimetallic oxalate bridged complex Rh_2(ox)$(COD)_2$ were synthesized by methods described below. In addition, the chemical oxidation reactions of selected complexes are also described.

TMA[Rh(ox)(COD)]·0.5CH_3CN

300 mg of [$Rh_2(\mu\text{-}Cl)_2(COD)_2$] (0.61mmol) and 153 mg of $H_2C_2O_4 \cdot 2H_2O$ (1.22 mmol) were dissolved in 20 ml of CH_3CN in a Schlenk flask. 2.44 mmol of tetramethylammonium hydroxide [(TMA)OH] dissolved in methanol/isopropanol were added and the resulting solution was evaporated to dryness under vacuum. The residue was dissolved in a minimum of methanol (about 2 ml) followed by the addition of a small quantity of acetonitrile (about 6 ml). Upon careful evaporation under vacuum, yellow crystals started to form. At this point a small amount of ether was added (about 1 ml) and the mixture was cooled in an ice bath. The resulting crystalline material was filtered, rinsed with cold acetonitrile, cold ether and dried under vacuum. Yield 65%. NMR $^{13}C\{^1H\}$ 100 MHz (CD_3OD): δ 170.0 (ox), 76.8 (cod=CH, d, J(Rh–C) 15 Hz), 56.0 (NMe_4^+), 31.5 (cod CH_2). ^1H 400 MHz (CD_3OD): δ 4.15 (br, cod=CH), 3.38 (NMe_4^+), 2.63 (br, cod–CH_2), 1.95 (pseudo d, J 8 Hz, cod–CH_2). IR (cm^{-1}) in CH_3CN: ν(COO) 1707(w), 1669(s), 1645(m).

TMA[Rh(ox)$(CO)_2$]

100 mg of [Rh(ox)(COD)] were dissolved in 5 ml of CH_3CN in a Schlenk flask and CO was slowly bubbled through the solution. The solution was cooled to −20 °C while CO was still being bubbled through the solution producing a green crystalline precipitate. The solid was filtered and rinsed with ether. Yield 60%. NMR $^{13}C\{^1H\}$ 100 MHz (CD_3OD): δ 185.1 (CO, d, J(Rh–C) 73 Hz), 167.8 (ox), 56.0 (NMe_4^+). IR (cm^{-1}) in CH_3CN: ν(CO) 2077, 2000, ν(COO) 1704, 1685, 1666; Nujol mull: ν(CO) 2068, 2002, ν(COO) 1703, 1667 (br).

[$Rh_2(ox)(COD)_2$]

A synthesis of this material has been previously reported [24]. An alternate synthesis is described here with spectroscopic data. To 250 mg of [$Rh_2(OCH_3)_2(COD)_2$] (0.52 mmol) and 20 ml of CH_2Cl_2, contained in a Schlenk flask, 65 mg of $H_2C_2O_4 \cdot 2H_2O$ (0.52 mmol) dissolved in 5 ml of methanol were added. The mixture was stirred until all of the solid dissolved. The volume was reduced and hexane was added producing a yellow solid which was filtered and rinsed with hexane. Yield 80%. NMR $^{13}C\{^1H\}$ 100 MHz ($CDCl_3$): δ 174.8 (ox), 77.0 (cod=CH, d, J(Rh–C) 64 Hz), 30.4 (cod CH_2). ^1H 400 MHz ($CDCl_3$): δ 4.08 (br, cod=CH), 2.41 (br, cod–CH_2), 1.69 (pseudo d, J 8 Hz, cod–CH_2). IR (cm^{-1}) in CH_2Cl_2: ν(ox) 1615(s), 1588(w).

Chemical oxidation of TMA[Rh(ox)(COD)]

A methanol solution of 65 mg of ferrocenium tetrafluoroborate, [$(Cp)_2Fe$]BF_4 (0.24 mmol), was added to a methanol solution of 100 mg of TMA[Rh(ox)(COD)] (0.24 mmol). The color of the ferrocenium ion instantly vanished and the resulting yellow–orange solution was evaporated to dryness under vacuum. The ferrocene that formed by the reduction of the ferrocenium ion was extracted with hexane, followed by the addition of methylene chloride to the remaining mixture. Insoluble (TMA)BF_4 was separated by filtration and the resulting rhodium product was precipitated by addition of hexane. IR and ^1H NMR spectra of the product were identical to pure samples of [$Rh_2(ox)(COD)_2$].

Chemical oxidation of [$Rh_2(ox)(COD)_2$]

54 mg of ferrocenium tetrafluoroborate, [$(Cp)_2Fe$]BF_4 (0.20 mmol), were added to 100 mg of [$Rh_2(ox)(COD)_2$] (0.20 mmol) in a 1:1 mixture of CH_2Cl_2/CH_3CN. The solution turned green indicating that a reaction had occurred. Chemical reaction is only observed in the presence of CH_3CN. The solvent was removed by vacuum and the product ferrocene was extracted three times with 5 ml of ether. The rhodium products were then extracted with CH_3CN to yield a bright green solution which was concentrated and then ether was layered into the solution. After 12 h at −20 °C, both a green solid and yellow crystals had formed. The yellow crystals were isolated and were determined to be [$Rh(CH_3CN)_2(COD)$]BF_4, based on IR and ^1H NMR data in the literature*. The green product was determined to be [$Rh_2(ox)(COD)_2(CH_3CN)$]BF_4, based on IR, NMR and elemental analysis. *Anal.* Calc. for [$Rh_2(ox)(COD)_2(CH_3CN)$]BF_4: C, 37.6; N, 2.15; H, 4.23. Found: C, 36.6; N, 2.12; H, 4.09%. IR analysis of the solid indicates the presence of $(BF_4)^-$, oxalate, COD and CH_3CN; in CH_2Cl_2 ν(COO) is 1621 cm^{-1}. NMR $^{13}C\{^1H\}$ 100 MHz (CD_3CN): 85.4 (cod=CH, d, J(Rh–C) 12 Hz), 30.6 (cod CH_2); 100 MHz(CD_3OD) 119.1 (CH_3CN), 81.8 (cod=CH, d, J(Rh–C) 13 Hz), 31.4 (cod CH_2), 1.3 (CH_3CN). ^1H 400 MHz (CD_3CN): δ 4.48 (br, cod=CH), 3.07 (s, CH_3CN), 2.56 (br, cod–CH_2), 1.98 (cod–CH_2); 400 MHz (CD_3OD), δ 4.35 (br, cod=CH), 3.14 (s, CH_3CN), 2.62 (br, cod–CH_2), 1.97 (cod–CH_2).

*The species [$Rh(COD)(S)_2$]$^+$ has been previously reported and characterized by IR and ^1H NMR [25].

Results and discussion

Synthesis and solution properties of (TMA)[Rh(ox)(COD)], (TMA)[Rh(ox)$(CO)_2$] and [$Rh_2(ox)(COD)_2$]

The reaction of [$Rh_2(\mu\text{-}Cl)_2(COD)_2$] with H_2ox and two equivalents of base yields either the monomeric [Rh(ox)(COD)]$^-$ or the bimetallic [$Rh_2(ox)(COD)_2$], depending on the molar ratio of [$Rh_2(\mu\text{-}Cl)_2(COD)_2$] to H_2ox used in the reaction. Formation of the CO complex, [Rh(ox)$(CO)_2$]$^-$, is accomplished by bubbling CO through solutions of [Rh(ox)(COD)]$^-$. The anion [Rh(ox)$(CO)_2$]$^-$, is strictly planar and the crystal structure of this species has been previously discussed [2]. The IR and NMR spectra of these complexes are all consistent and in conjunction with the crystallographic data for [Rh(ox)$(CO)_2$]$^-$ demonstrate that Rh(I) is in a square planar arrangement for all three complexes. This is shown in Scheme 1.

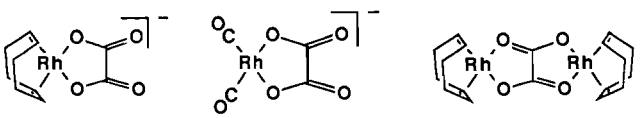

Scheme 1.

While the monomeric species have spectra that are relatively independent of the solvent used, a similar result is not found for [$Rh_2(ox)(COD)_2$]. For example, the solution IR spectra of [$Rh_2(ox)(COD)_2$] in weak coordinating solvents such as CH_2Cl_2 or ether are dominated by a strong absorption near 1615 cm^{-1} due to the oxalate ligand. However in CH_3CN, the spectrum is relatively complex with bands found at 1706(w), 1669(s), 1623(s) and 1593(w) cm^{-1}. This suggests reaction of the bimetallic species with coordinating solvents is possible and in fact the observed spectrum is due to the presence of an equilibrium between [$Rh_2(ox)(COD)_2$], [Rh(ox)(COD)]$^-$ and [Rh(COD)$(CH_3CN)_2$]$^+$ as shown in eqn. (1).

$$[Rh_2(ox)(COD)_2] \overset{2CH_3CN}{\rightleftharpoons} [Rh(ox)(COD)]^- + [Rh(COD)(CH_3CN)_2]^+ \quad (1)$$

The bands at 1706 and 1669 cm^{-1} correspond to the monomeric compound $[Rh(ox)(COD)]^-$, while the weak band at 1593 cm^{-1} is due to the bimetallic species. The broad absorption at 1623 cm^{-1} is due to the addition of a monomeric band at 1645 cm^{-1} and the bimetallic species band at 1615 cm^{-1}. This is shown in Fig. 1, which gives IR spectral data for the monomer CH_3CN (Fig. 1(a)), the bimetallic species in CH_2Cl_2 (Fig. 1(b)) and the bimetallic species in CH_3CN (Fig. 1(c)).

Electrochemistry of (TMA)[Rh(ox)(COD)] and (TMA)[Rh(ox)(CO)$_2$]

Figure 2(a) is representative of multiple scan, cyclic voltammetric data obtained for (TMA)[Rh(ox)(COD)] in THF/TBAP at a scan rate of 100 mV/s. One broad oxidation wave is found at $E_{pa} = 0.78$ V versus SCE (wave 1, Fig. 2(a)) without any indication of a reduction wave that would suggest a chemically reversible process. In addition, no reduction processes are found when the potential is scanned in a negative direction up to -2.2 V versus SCE.

Wave analysis data for wave 1 for (TMA)-[Rh(ox)(COD)] are summarized in Table 1. Analysis of wave 1 suggests that it is a diffusion controlled process, but the value of $E_p - E_{p/2}$ of 100 mV is too large for a simple one-electron transfer reaction [26, 27]. This is due to the presence of an EC or ECE electron transfer process* which is demonstrated by the spectral data (*vide post*). Furthermore, the cyclic voltammetric data are consistent with an overall EC or ECE mechanism. A very small reduction process centered around -0.5 V versus SCE (wave 1', Fig. 2(a)) is also observed in Fig. 2(a). This wave is not present if the potential is not scanned positive of wave 1 and multiple scans in the cyclic voltammetric experiments that do not sweep to potentials negative of

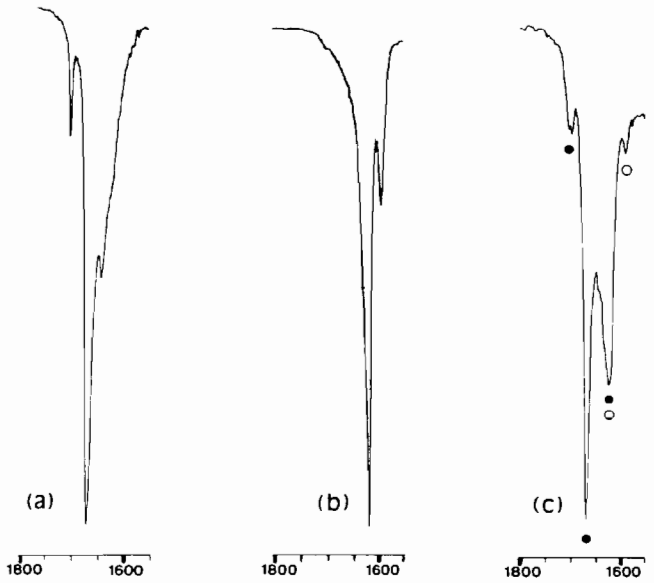

Fig. 1. IR data for: (a) (TMA)[Rh(ox)(COD)] in CH_3CN, (b)[Rh_2(ox)$(COD)_2$] in CH_2Cl, (c) [Rh_2(ox)$(COD)_2$] in CH_3CN. Bands marked ○ correspond to [Rh_2(ox)$(COD)_2$]; ● correspond to $[Rh(ox)(COD)]^-$.

*E signifies an electron transfer and C signifies a coupled chemical reaction; see refs. 26 and 27 for details.

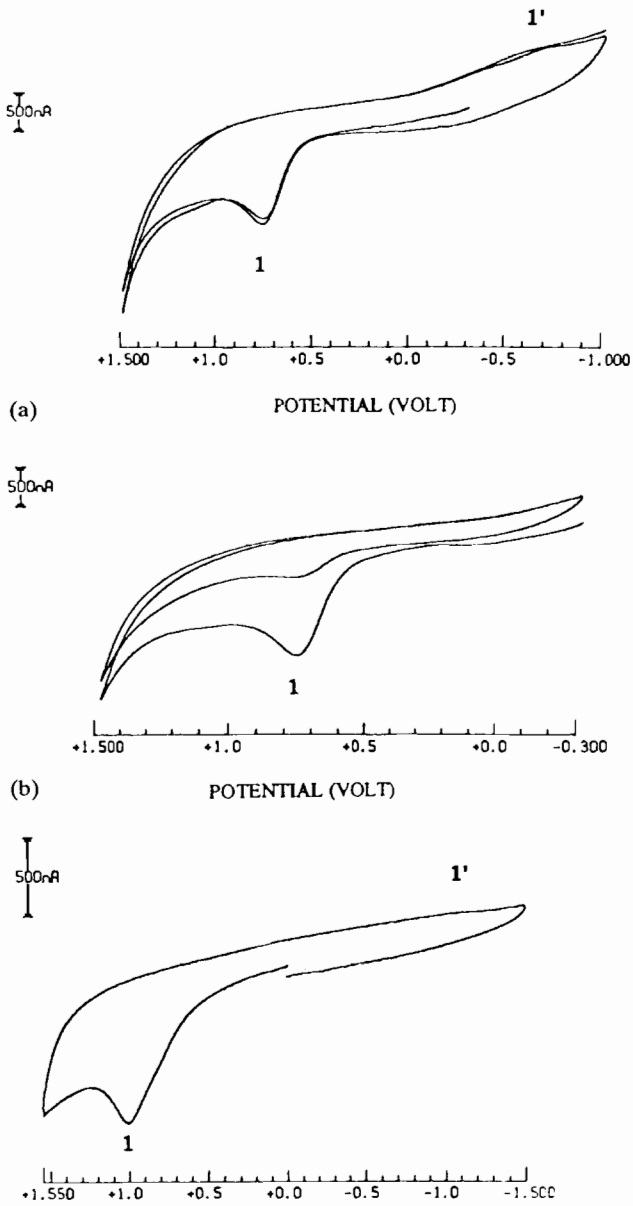

Fig. 2. (a) Multiple scan cyclic voltammogram of a 2 mM solution of (TMA)[Rh(ox)(COD)] in THF, 0.20 M TBAP, potential range 1.50 to -1.00 V. Scan rate of 100 mV/s. (b) same as (a), potential range 1.50 to -0.30 V. Note the passivation of the electrode. (c) Cyclic voltammogram of a 2.0 mM solution of (TMA)[Rh(ox)$(CO)_2$] in THF, 0.2 M TBAP, potential range 1.55 to -1.50 V. Scan rate of 100 mV/s.

TABLE 1. Electrochemical wave analysis of rhodium complexes

Compound	Solvent[a]	Wave	E_p[b]	$E_p - E_{p/2}$[c]	$i_p/v^{1/2}$	E_{pa} (Fc)[d]
$[Rh(ox)(COD)]^-$	THF	1	0.78	100	constant	0.62
	CH_3CN	1	0.58	120	constant	0.49
	CH_2Cl_2	1	0.81	[e]	[e]	0.60
$[Rh(ox)(CO)_2]^-$	THF	1	1.09	[e]	[e]	0.73
	CH_3CN	1	0.78	[e]	[e]	0.44
	CH_2Cl_2	1	0.92	[e]	[e]	0.42
$[Rh_2(ox)(COD)_2]$	THF	1	1.20	95	constant	0.64
	THF	2	1.38	80	constant	0.64
	CH_3CN	1	0.75	110	constant	0.39
	CH_3CN	2	1.10	100	constant	0.39
	CH_2Cl_2	1	1.01	[e]	[e]	0.45
	CH_2Cl_2	2	1.13	[e]	[e]	0.45

[a]TBAP as supporting electrolyte. [b]Volts vs. SCE, scan rate of 100 mV/s. [c]Millivolts, scan rate of 100 mV/s. [d]Value of E_{pa} in volts vs. SCE for ferrocene added as an internal standard. [e]Peak not well defined; see text.

wave 1′ show rapid passivation of the electrode surface. This is shown in Fig. 2(b). These data demonstrate that the product of the oxidation of (TMA)-[Rh(ox)(COD)] (wave 1) passivates the electrode surface, but this surface effect can be removed by scanning to potentials negative of wave 1′.

The electrochemical response for (TMA)[Rh(ox)-(COD)] when acetonitrile is the solvent is basically the same as that found for THF and the electrochemical data are summarized in Table 1. The major difference with the change in solvent is that wave 1 shifts to $E_{pa} = 0.58$ V versus SCE at a scan rate of 100 mV/s. This shift implies participation of acetonitrile in the chemical reaction following electron transfer [1, 28, 29], such as coordination to the reaction products.

Cyclic voltammetric data for (TMA)[Rh(ox)$(CO)_2$] is qualitatively the same as that found for (TMA)[Rh(ox)(COD)]. As an example, Fig. 2(c) shows the electrochemical response for the dicarbonyl adduct with THF as the solvent system. Only one oxidation wave is found (wave 1, Fig. 2(c)) at 1.09 V versus SCE, with the presence of a small reduction wave centered at −1.00 V versus SCE (wave 1′, Fig. 2(c)) at a scan rate of 100 mV/s. The location of wave 1 for (TMA)[Rh(ox)$(CO)_2$] is shifted 310 mV positive of the oxidation potential for the COD adduct, fully consistent with the greater π acidity of the CO ligands. Passivation of the electrode surface is observed on the second and subsequent scans in the multiple scan cyclic voltammetric data if the potential is not scanned negative of wave 1′. Wave analysis data for the oxidation of (TMA)[Rh(ox)$(CO)_2$] are summarized in Table 1, and are consistent with a diffusion controlled process with coupled chemical steps.

Thin layer experiments show that while process 1′ eliminates the surface effects caused by the oxidation of (TMA)[Rh(ox)$(CO)_2$], the starting material is not regenerated by this process. Hence under these diffusion limited conditions, multiple scan data show a rapid decrease in the concentration of (TMA)[Rh(ox)(COD)] around the electrode surface with each oxidation–reduction cycle. That wave 1 is observed unchanged in the multiple scan cyclic voltammograms (such as Fig. 2(a)) is due to diffusion of new material to the electrode surface during the time the potential of the electrode is scanned at potentials less positive than wave 1.

Bulk electrolysis studies were performed on (TMA)[Rh(ox)(COD)] and (TMA)[Rh(ox)$(CO)_2$] to determine the number of electrons transferred in the process associated with wave 1. To minimize the surface effects, the bulk electrolysis experiments were performed at substantially lower concentrations, via injection of a known amount of compound after the background current decayed to baseline levels. The number of electrons transferred per rhodium was found to be 2.02 ± 0.14 and 2.00 ± 0.27 for the COD and CO complexes, respectively.The large error in each case is due to the use of small quantities of the complex. However, the oxidation of (TMA)[Rh(ox)(COD)] and (TMA)-[Rh(ox)$(CO)_2$] are both best described as two electron processes, with coupled irreversible chemical reactions.

Figure 3(a) and (b) is representative of the IR spectroelectrochemical results for (TMA)[Rh(ox)-(COD)] with CH_2Cl_2 as the solvent. The starting material is characterized by a strong ν(COO) stretch for the oxalate at 1660 cm^{-1} and two overlapping shoulders centered at 1625 cm^{-1} (Fig. 3(a)). Upon oxidation at potentials positive of wave 1 these bands decrease to baseline. At the same time a small band at 1600 cm^{-1} is formed. This band may be real, but is suspect due to the low intensity. Application of a potential negative

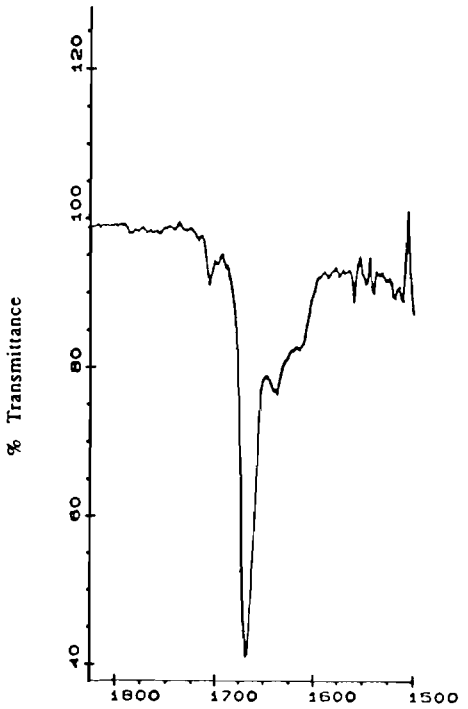

(a)

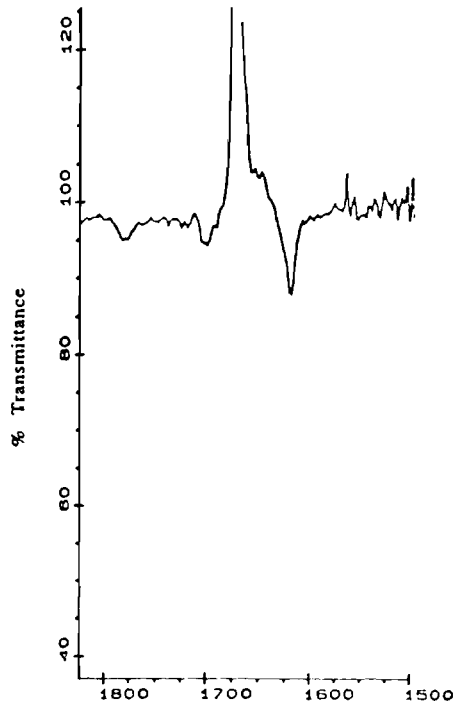

(b)

Fig. 3. (a) IR data for 3 mM (TMA)[Rh(ox)(COD)] in CH_2Cl_2, 2.0 M TBAP. (b) IR spectral changes upon oxidation at 1.5 V vs. Pt wire reference in the spectral range of 1825 to 1500 cm^{-1}.

of wave 1′ to solutions of the oxidized compound do not show any significant change in the IR spectrum.

The spectroelectrochemical data for (TMA)-$[Rh(ox)(CO)_2]$ are similar to those found for the COD adduct in that oxidation results in irreversible changes in the spectral data. Furthermore, there appears to be a total loss of bands in the regions monitored, including the ν(CO) stretching bands at 2000 and 2076 cm^{-1} for the metal carbonyl chromophores.

Based on the results reported for oxalate compounds [12–16] and on the IR spectroelectrochemical data, the electron transfer reactions for these two compounds are best described as a two-electron oxidation with coupled chemical reactions that include decomposition of the oxalate ligand. This is the case since the IR bands due to the coordinated oxalate decrease to the background while free oxalate is not observed. Under our conditions free oxalate is observed in the IR at ν(COO) of 1710 cm^{-1} (measured in our laboratory). No indication was found in the IR data for an absorption in that region. For (TMA)[Rh(ox)(COD)] the formation of $[Rh(COD)(S)_2]^+$ is observed upon chemical oxidation (see next section) and this is shown in Scheme 2.

The oxidation is best described as removal of two electrons from either $[Rh(ox)(CO)_2]^-$ or $[Rh(ox)(COD)]^-$ to generate a formal rhodium(III) center. This would then be able to undergo a reductive elimination of oxalate, regenerating the Rh(I) center and two equivalents of CO_2. The formal potential for the oxidation of oxalic acid is 0.475 V versus NHE [18] and in a non-aqueous system the oxidation shifts to significantly more positive potentials. For example in 0.2 M TBAP CH_3CN we find a broad oxidation wave centered at $E_p = 1.57$ V versus SCE for oxalic acid by square wave voltammetry. The potential for the reduction of Rh(III) to Rh(I) is highly ligand dependent and ligation by either COD or two equivalents of CO would favor formation of an Rh(I) species. Hence, the energetics are reasonable for the reductive elimination of oxalate from the electrogenerated Rh(III) center. The nature of the species that passivates the electrode surface is unknown.

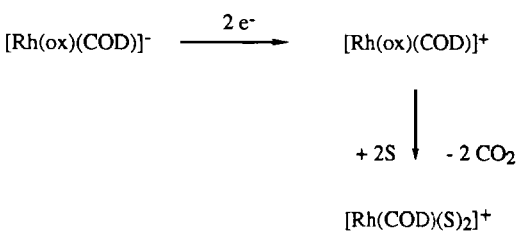

Scheme 2.

Chemical oxidation of (TMA)[Rh(ox)(COD)]

Chemical oxidation studies were performed on (TMA)[Rh(ox)(COD)] as described in 'Experimental'. When one equivalent of the oxidant was added, the product was found to be the bimetallic species $[Rh_2(ox)(COD)_2]$ as shown in eqn. (2).

$$2(TMA)[Rh(ox)(COD)] + 2[(Cp)_2Fe]BF_4 \longrightarrow [Rh_2(ox)(COD)_2] + 2(Cp)_2Fe + 2TMA(BF_4) + 2CO_2 \quad (2)$$

This is in complete agreement with the electrochemical data for $[Rh(ox)(COD)]^-$, considering the presence of the equilibrium described by eqn. (1). Hence when one equivalent of oxidant is added, half of the $[Rh(ox)(COD)]^-$ present is oxidized to form $[Rh(COD)(S)_2]^+$ which then reacts with the remaining $[Rh(ox)(COD)]^-$ to form the bimetallic species $[Rh_2(ox)(COD)_2]$.

Chemical oxidation of $[Rh(ox)(COD)]^-$ with an excess of $K_2Ce(NO_3)_6$ in acetonitrile was also performed and in this case analysis of the resulting product by IR demonstrated no bands in the ν(COO) region for oxalate. This is consistent with the spectroelectrochemical data and with Scheme 2. Furthermore, new bands at 2407 and 2373 cm^{-1} were found in the IR that we assign to the nitrile stretch of acetonitrile coordinated to the resulting rhodium product. $[Rh(COD)(CH_3CN)_2]^+$ was reported to have two bands at 2320 and 2290 cm^{-1} [25] while free acetonitrile has two nitrile stretching bands at 2298 and 2250 cm^{-1} (measured in our laboratory). The larger shift to higher wavenumbers implies that our product generated in the presence of excess ceric ion has been further oxidized, presumably to an Rh(III) species based on the magnitude of the shift in ν(CN) [30]. Hence there is a total loss of oxalate and formation of a solvated rhodium product upon complete oxidation of $[Rh(ox)(COD)]^-$ with ceric ion.

Electrochemistry of $[Rh_2(ox)(COD)_2]$

Figure 4(a) is representative of the cyclic voltammetric response for $[Rh_2(COD)_2(ox)]$ in CH_3CN. In this case two oxidation waves are observed at $E_{pa} = 0.75$ V versus SCE (wave 1, Fig. 4(a)) and at $E_{pa} = 1.10$ V versus SCE (wave 2, Fig. 4(a)) at 100 mV/s. No re-reduction waves are observed for either wave up to scan rates of 1000 mV/s that would suggest a chemically reversible process. In addition, no return wave is found for wave 1 if the potential scan is reversed between waves 1 and 2. However, there is a small reduction wave near −0.100 V versus SCE (wave 1', Fig. 4(a)). No reduction waves are found for this complex up to −2.2 V versus SCE.

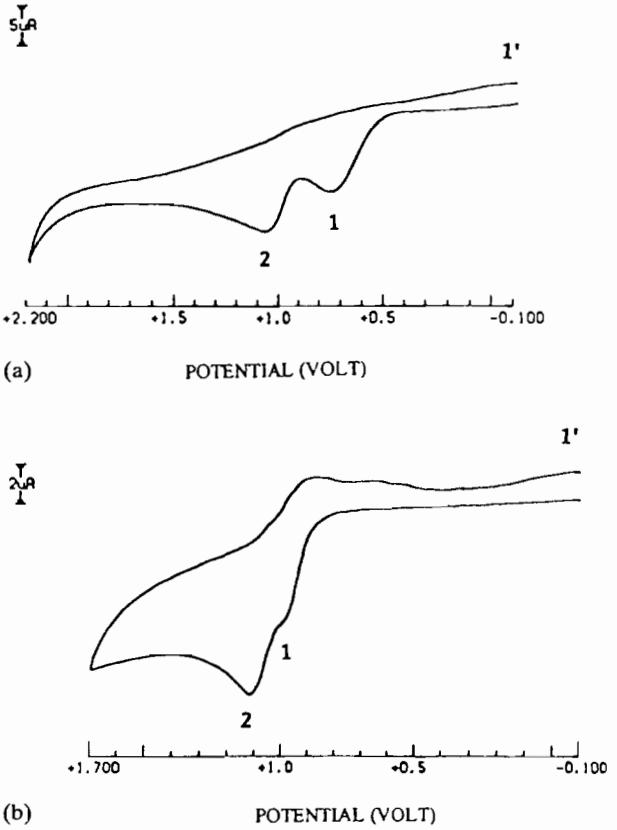

Fig. 4. (a) Cyclic voltammogram of a 2.0 mM solution of $[Rh_2(ox)(COD)_2]$ in CH_3CN, 0.20 M TBAP. Scan rate of 100 mV/s. (b) Cyclic voltammogram of a 2.0 mM solution of $[Rh_2(ox)(COD)_2]$ in CH_2Cl_2, 0.20 M TBAP. Scan rate of 100 mV/s.

Wave analysis data for waves 1 and 2 are summarized in Table 1. In both cases, the data suggest that the electron transfer reactions contain coupled, irreversible chemical reactions. Multiple scan cyclic voltammograms do not show passivation of the electrode surface, in contrast to the data obtained for the monomeric complexes. Bulk electrolysis of this compound at potentials positive of wave 2 give a total of 3.87 ± 0.13 electrons transferred per mole of $[Rh_2(ox)(COD)_2]$. Given that the peak height for waves 1 and 2 are approximately equal, the bulk electrolysis data suggest that two electrons are transferred in each step, for the total of four electrons.

The electrochemistry of $[Rh_2(ox)(COD)_2]$ has a strong dependence on the solvent system. This is shown in Fig. 4(b), which represents the cyclic voltammetric response when the solvent is CH_2Cl_2. In addition to a general positive shift in the oxidation potential, waves 1 and 2 are now overlapping processes. They occur at $E_{pa} = 1.01$ V versus SCE (wave 1, Fig. 4(b)) and at 1.13 V versus SCE (wave 2, Fig. 4(b)) at a scan rate of 100 mV/s. In addition to observing wave 1' at 0.00 V versus SCE, there are small re-reduction waves at

$E_{pc} = 0.90$ and 0.60 V versus SCE at 100 mV/s. The electrochemical data for this complex as a function of solvent are summarized in Table 1. The dependence of the electrochemistry on the solvent suggests that acetonitrile stabilizes the formal Rh(II), Rh(II) complex presumably by coordination after oxidation. Stabilization of Rh(II) by acetonitrile has been reported in the literature [31, 32]. On the other hand, the reaction of electrogenerated Rh(II) complexes with methylene chloride and other alkyl halides to generate a rhodium–alkyl species is also known [33, 34] and such a reaction could also account for the different electrochemical behavior.

The UV–Vis spectroelectrochemical data for this complex was completed. The original complex is characterized by bands at 223, 268 and 374 nm in CH_2Cl_2, which upon oxidation at a potential positive of wave 2 decrease in intensity. At the same time new bands are found at 210 and 260 nm as shown in Fig. 5(a). When a potential negative of wave 1′ is applied to solutions of the oxidized species, the original spectrum is regenerated, as shown in Fig. 5(b), suggesting that on the spectroelectrochemical timescale the chemical reactions following electron transfer can be reversed. Hence, a reductive elimination of oxalate to CO_2 *does not* occur when the bimetallic species is oxidized, unlike the monomeric species. Similar spectroelectrochemical data are obtained when CH_3CN is used as the solvent. Since the spectroelectrochemical data are similar in both solvents, the solvent dependence of the cyclic voltammetric response is probably due to a stabilization of the oxidized rhodium product by CH_3CN rather than distinct chemical reactions with CH_3CN and CH_2Cl_2.

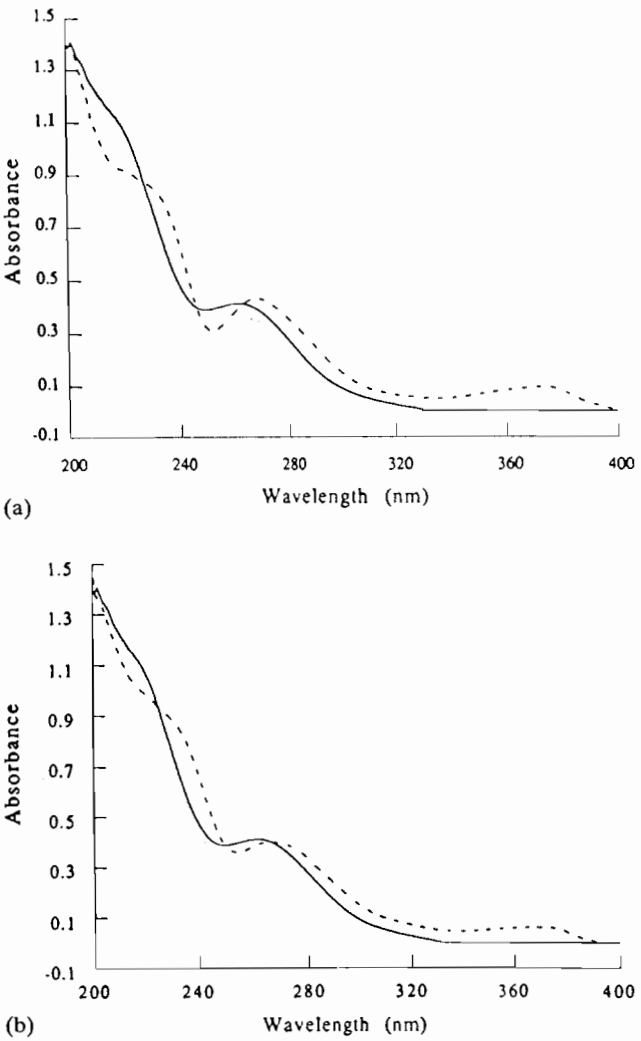

Fig. 5. Spectroelectrochemical data for 3.5 mM $Rh_2(ox)(COD)_2$ in 0.2 M TBAP, CH_2Cl_2. (a) Oxidation at 1.50 V vs. Pt wire reference; initial complex (– – –), oxidation product (——) in the spectral range of 360 to 210 nm. (b) Re-reduction at −1.20 V vs. Pt wire reference; oxidized complex (——), reduction product (– – –) in the spectral range of 360 to 210 nm.

Chemical oxidation of $[Rh_2(ox)(COD)_2]$

The chemical oxidation of $[Rh_2(ox)(COD)_2]$ with $[(Cp)_2Fe]BF_4$ was attempted and in the absence of acetonitrile no reaction was observed. However, when the reaction was performed in the presence of acetonitrile, formation of $[Rh(COD)(CH_3CN)_2]BF_4$ and a species with the composition $[Rh_2(ox)(CH_3CN)(COD)_2]BF_4$ was determined. The solvated species was determined by comparison with literature data [25], while $[Rh_2(ox)(CH_3CN)(COD)_2]BF_4$ is a new product.

The elemental analysis and spectral data for $[Rh_2(ox)(CH_3CN)(COD)_2]BF_4$ are in close agreement. The coordinated acetonitrile is assigned to the resonance near 3.00 ppm in the ^1H NMR spectra and to resonances at 119.1 and 1.3 ppm in the proton decoupled ^{13}C NMR. The structure of this complex is difficult to assign since charge balance indicates an Rh(I)–Rh(II) complex. However, the NMR indicates that the product is diamagnetic. One possibility is for two of the Rh(I)–Rh(II) units to form a Rh(II)–Rh(II) bond and hence produce a diamagnetic unit. However, other possibilities exist as well.

Based on the cyclic voltammetric data, $[(Cp)_2Fe]BF_4$ should not be a strong enough oxidant to abstract electrons from $[Rh_2(ox)(COD)_2]$. However, that the oxidation by $[(Cp)_2Fe]BF_4$ is only observed in the presence of acetonitrile suggests that the oxidation reaction is not with $[Rh_2(ox)(COD)_2]$ but rather between the $[(Cp)_2Fe]^+$ and the product of the reaction between $[Rh_2(ox)(COD)_2]$ and acetonitrile. In fact, this oxidation reaction has trapped an intermediate in the dissociation reaction of the bimetallic species (eqn. (1)). Hence, isolation of $[Rh_2(ox)(CH_3CN)(COD)_2]BF_4$ demonstrates that addition of acetonitrile occurs prior to dissociation of the bimetallic species as expected for a square planar complex. The addition of the acetonitrile

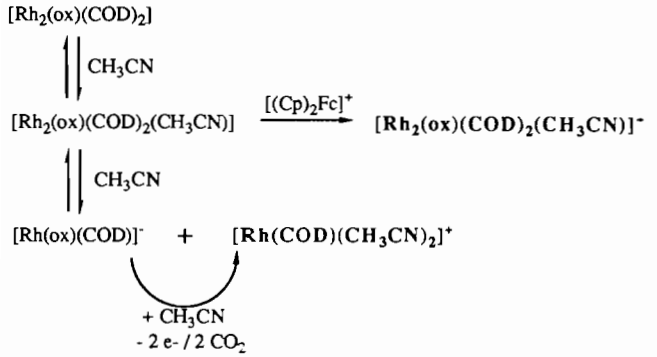

Scheme 3.

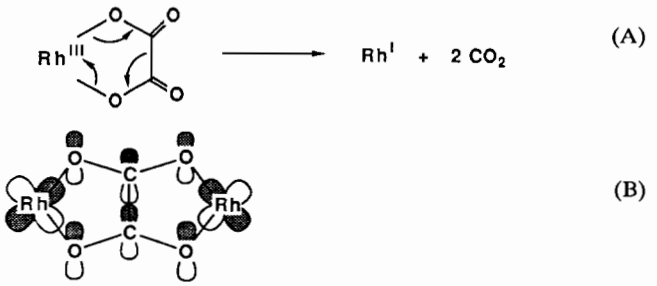

Scheme 4.

to one of the rhodium atoms lowers the oxidation potential of the product allowing oxidation to occur, as outlined in Scheme 3. The other product formed in the oxidation reaction is $[Rh(COD)(CH_3CN)_2]^+$, which is both the two-electron oxidation product of $[Rh(ox)(COD)]^-$ and one product of the dissociation reaction of the bimetallic species. Hence the observed products (in bold in Scheme 3) are $[Rh(COD)(CH_3CN)_2]^+$ and $[Rh_2(ox)(COD)_2(CH_3CN)]^+$.

Discussion

It is interesting to speculate on whether the first oxidation process for $[Rh_2(ox)(COD)_2]$ (wave 1, Fig. 4(a)) generates an Rh(II),Rh(II) species or an Rh(III),Rh(I) mixed valence species. We believe that the Rh(II),Rh(II) complex is formed or that the two metal centers are strongly coupled. A strong coupling of metal centers with oxalate complexes has been previously reported. For example, oxalate has been shown to form magnetically coupled dimers and chains with copper(II) systems [35, 36] indicative of the 'communication' that occurs across the oxalate molecule. However, the UV–Vis spectroelectrochemical data *do not* discriminate between the two possibilities since an intervalence charge transfer band was not observed.

The mechanism for reductive elimination of oxalate from the monomer is given in Scheme 4, part A where the non-oxalate ligands bonded to the rhodium are not drawn. There is a two-electron transfer from oxalate to the rhodium followed by electron rearrangement to give two equivalents of CO_2. The product of the oxidation of $[Rh_2(ox)(COD)_2]$ is not known, but the reversibility of the process is surprising. It was anticipated that the bimetallic species would reductively eliminate CO_2 following oxidation, similar to the two monomeric species. The increased stability of the oxalate ligand in the bimetallic species towards reductive elimination is clearly due to the presence of the second rhodium atom. If resonance structures are ignored, then the filled d_{xz} or d_{yz} orbitals of the second rhodium(III) atom can form a five-membered ring with a total of six π electrons. This is an aromatic system that would stabilize the carbon–carbon bond of the oxalate ligand, and presumably increase the energy necessary for reductive elimination. This is shown in Scheme 4, part B where again the non-oxalate ligands bonded to the rhodium center are not drawn.

Acknowledgements

J.E.A. acknowledges Johnson Matthey for the loan of rhodium metal. J.C.B. acknowledges financial support from the Spanish DGICYT (PB-88-0252).

References

1 J. E. Anderson, T. P. Gregory, G. Net and J. C. Bayón, *J. Chem. Soc., Dalton Trans.*, (1992) 487.
2 J. Real, J. C. Bayón, F. J. Lahoz and J. A. López, *J. Chem. Soc., Chem. Commun.*, (1989) 1889.
3 P. G. Rasmussen, J. E. Anderson, O. H. Bailey, M. Tamres and J. C. Bayón, *J. Am. Chem. Soc., 107* (1985) 279.
4 P. G. Rasmussen, J. B. Kolowich and J. C. Bayón, *J. Am. Chem. Soc., 110* (1988) 7042.
5 J. C. Bayón, G. Net, P. G. Rasmussen and J. B. Kolowich, *J. Chem. Soc., Dalton Trans.*, (1987) 3003.
6 J. C. Bayón, G. Net, P. Esteban, P. G. Rasmussen and D. F. Bergstrom, *Inorg. Chem., 30* (1991) 4771.
7 R. L. Cowan, D. B. Pourreau, A. L. Rheingold, S. J. Geib and W. C. Trogler, *Inorg. Chem., 26* (1987) 259.
8 R. S. Paonessa, A. L. Prignano and W. C. Trogler, *Organometallics, 4* (1982) 647.
9 D. A. Freedman and K. R. Mann, *Inorg. Chem., 30* (1991) 836.
10 T. D. Waite and F. M. M. Morel, *J. Colloid. Interface Sci., 102* (1984) 121.
11 M. A. Blesa, H. A. Marinovich, E. C. Baumgartner and A. J. G. Maroto, *Inorg. Chem., 26* (1987) 3713.
12 D. A. Skoog and D. M. West (eds.), *Fundamentals of Analytical Chemistry,* Saunders, New York, 4th edn., 1982, p. 369.
13 R. P. Farrell, R. J. Judd, P. A. Lay, R. Bramley and J.-Y. Ji, *Inorg. Chem., 28* (1989) 3403.
14 M. Krumpolic and J. Rocek, *J. Inorg. Chem., 24* (1985) 617.
15 M. Mitewa and R. Bontchev, *Coord. Chem. Rev., 61* (1985) 214.
16 C. R. Steffan, A. Bakac and J. H. Espenson, *Inorg. Chem., 28* (1989) 2992.

17 A. Bakac, K. Zahir and J. H. Espenson, *J. Am. Chem. Soc., 110* (1988) 5059.
18 A. J. Bard, R. Parsons and J. Jordan (eds.), *Standard Potentials in Aqueous Solution,* Marcel Dekker, New York, 1985, p. 195.
19 J. E. Anderson and T. P. Gregory, *Inorg. Chem., 28* (1989) 3905.
20 J. E. Anderson, S. M. Sawtelle and C. E. McAndrews, *Inorg. Chem., 29* (1990) 2627.
21 D. Shriver and M. A. Drezdzon, *The Manipulation of Air Sensitive Compounds,* Wiley, New York, 2nd edn., 1986.
22 J. A. Riddick, W. B. Bunger and T. K. Sakano, *Organic Solvents,* Interscience–Wiley, New York, 4th edn., 1986.
23 R. Uson, L. A. Oro and J. A. Cabeza, *Inorg. Synth., 23* (1985) 126.
24 L. A. Oro, M. T. Pinillos and M. P. Jarauta, *Polyhedron, 4* (1985) 325.
25 M. Green, T. A. Kuc and H. Taylor, *J. Chem. Soc A,* (1971) 2334.
26 A. J. Bard and L. R. Faulkner, *Electrochemical Methods, Fundamentals and Applications,* John Wiley and Sons, New York, 1980.
27 R. S. Nicholson and I. Shain, *Anal. Chem., 36* (1964) 706.
28 K. M. Kadish, *Prog. Inorg. Chem., 34* (1986) 435.
29 S. Kelly and K. M. Kadish, *Inorg. Chem., 23* (1984) 679.
30 F. A. Cotton and G. Wilkinson, *Advanced Inorganic Chemistry,* Wiley, New York, 4th edn., 1980, p.82.
31 K. R. Dunbar, *J. Am. Chem. Soc., 110* (1988) 8247.
32 T.R. Felthouse, *Prog. Inorg. Chem., 29* (1982) 73.
33 J. E. Anderson, C.-L. Yao and K. M. Kadish, *Inorg. Chem., 25* (1986) 718.
34 J. E. Anderson, C.-L. Yao and K. M. Kadish, *J. Am. Chem. Soc., 109* (1987) 1106.
35 U. Geiser, B. L. Ramakrishna, R. D. Willett, F. B. Hulsberger and J. Reedijk, *Inorg. Chem., 26* (1987) 3750.
36 M. Julve, M. Verdaguer, O. Kahn, A. Gleizes and M. Philoche-Levisalles, *Inorg. Chem., 22* (1983) 368.